Altermagnetism in MnTe: Origin, predicted manifestations, and routes to detwinning

I. I. Mazin

Phys. Rev. B **107**, L100418 — Published 27 March 2023

DOI: 10.1103/PhysRevB.107.L100418

Altermagnetism in MnTe: origin, predicted manifestations, and routes to detwinning

I. I. Mazin
Department of Physics and Astronomy, George Mason University, Fairfax, VA 22030, USA and Quantum Science and Engineering Center, George Mason University, Fairfax, VA 22030, USA

MnTe has recently attracted attention as an altermagnetic candidate. Experimentally it has an altermagnetic order of ferromagnetic *ab* planes, stacked antiferromagnetically along *c*. We show that this magnetic order (by itself non-trivial, since the in-plane exchange in antiferromagnetic) opens intriguing possibility of manufacturing altermagnetically-detwinned samples and generate observable magnetooptical response (which we calculate from first principles) as a signature of altermagnetism.

The recently discovered phenomenon of spin-split bands in collinear symmetry-compensated antiferromagnets, dubbed "altermagnetism" (AM)[1–3], has attracted considerable attention. While a number of altermagnets have been theoretically identified, there is a big experimental challenges in assessing this, for a number of reasons: First, most of them are not metals, so anomalous Hall conductivity cannot be measured. Second, many have the easy magnetization direction not compatible with anomalous response. Third, statistically these materials form chiral domains, so that the anomalous response of opposite signs largely cancels.

There are ways to overcome these difficulties. First, since the nondiagonal optical conductivity, accessible through magnetooptical effects, is governed by the same selection rules as the anomalous Hall conductivity, it can be used in its place to detect the AM response. An additional advantage is that, as discussed later in the paper, calculations of the finite-frequency response from the first principles is mush easier and more reliable than in the static (Hall) limit. Finally, while the chiral domains necessarily form statistically, as the magnetic phase is nucleating upon cooling, simultaneously in different parts of the sample, this does not carry, as opposed to ferromagnets, any energy advantage, only the energy cost of forming domain walls. This suggests that carefull annealing through the Neel temperature, preferably with a temperature gradient, in order to suppress independent nucleation in different parts of the sample, or on a ferromagnetic substrate, in order to encourage a single domain on the interface, may result in a single domain sample, or domains large enough to be probed by polarized light independently. However, before urging experimentalists to pursue this path, a better and more quantitative understanding of this material is imperative.

Specifically, two main issues need to be understood: (i) magnetic interactions in MnTe, as they eventually determing the domain wall dynamics, and (ii) frequencies at which the strongest magnetoptical response is expected, and an estimate of the latter. In this paper we will provide both.

MnTe crystallizes in the NiAs crystal structure, as is known since 1956[4], which can be viewed as the hexagonal analog of the metastable cubic MnTe (crystallized in the NaCl structure)[5]. In the latter, both Mn and O form triangular layers stacked along (111) as AbCaBc (the uppercase letters correspond to the Mn layers). In the former, the stacking sequence is AbAc, and the structure is expanded in the direction perpendicular to the triangular planes, and squeezed in the planes (Fig. 1). As a

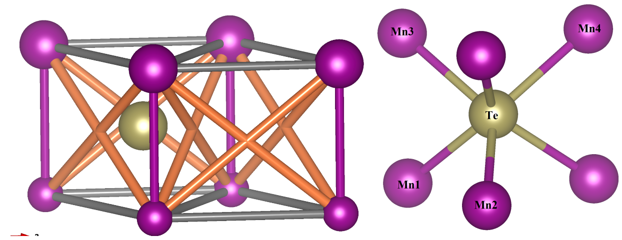

FIG. 1. Crystal structure of MnTe. The purple/gray/orange bonds connect 1st/2nd/3rd neighbors. The Mn1-Te-Mn3 angle is 70.3°, the Mn1-Te-Mn2 one 90.1°, and the Mn2-Te-Mn3 one 131.7°

result, while the Mn-Mn interlayer distance is 2.60 Å in the cubuc MnTe, it is 3.37 Å in the hexagonal one, which is also the shortest Mn-Mn bond. The next bond connects two Mn in the *ab* plane, and is 4.15 Å long; both are shorter than the corresponding bonds in the cubic material, which is 4.23 Å. The corresponding Mn-Te-Mn angles (Fig. 1) are 70.3° and 90.1°. The third neighbors correspond to the second neighbors in the cubic structure, where they are bridged by Te along the straight line (a 180° angles) and the distance is 5.98 Å; in the hexagonal structure it is 5.35 Å and the angle is 131.7°.

MnTe has been studied a lot, both experimentally and theoretically. The latest and the most comprehensive study was probably Ref. [6] (see also the references therein). Experimentally, there is full consensus that MnTe forms an A-type antiferromagnetic structure with $\mathbf{q} = (0, 0, 0)$, and the magnetic moments are collinear and aligned with the (210) direction (i.e., perpendicular to a Mn-Mn bond; here and below all directions are given in the units of the lattice vectors in the standard setting). The in-plane magnetic anisotropy energy K was found to be too small to be measured by neutrons in Ref. [7], and too small to be calculated reliably in Ref. [6]. The in-plane spin-flop field, $\mu_B H_{sf} \approx \sqrt{2KJ}$, in Ref. [6] was between 2 and 6 T, which, using the leading exchange coupling of $J \sim 40$ meV (see below), corresponds to $K \approx 0.2 - 1.4\ \mu$eV.

Spin-wave dispersion was fitted with three nearest neighbor Heisenberg exchange coupling, defined via the Hamiltonian

$$H = \sum_{i=1-3} J_i \hat{\mathbf{m}} \cdot \hat{\mathbf{m}}', \quad (1)$$

where the summation is over all different bonds of a given length, and $\hat{\mathbf{m}}$, $\hat{\mathbf{m}}'$ are the unit vectors of spins forming the bond. The resulting parameters are listed in Table 1, together with those calculated in Ref. [8] and our own calculations. Note that both DFT calcula-

TABLE I. Calculated and experimental Heisenberg exchange parameters, in meV, as well as the Curie-Weiss temperatures.

	J_1	J_2	J_3	J_4	T_{CW} (K)
Expt. ([7])	46.2	-1.44	6.2	-	612^a, 585^b
Calc. ([8])	38.4	0.34	5.0	2.0	552
Calc. (this work)	42.1	0.91	5.3	-	592

^{a} calculated from the exchange parameters in Ref. [7].
^{b} measured[9, 10].

tions, while performed by different methods (VASP[11] in Ref. [8], LAPW[12] here), give the nearest-neighbor in-plane exchange J_2 antiferromagnetic, while Ref. [7] reports a very small ferromagnetic value. We believe that this is an experimental artifact, maybe due to neglect of the longer interactions in the spin-wave analysis. Indeed, for Mn^{2+} there is no superexchange mechanism that could generate a ferromagnetic coupling, and no itinerant electrons to promote ferromagnetism. Since the bond angle in this case is nearly exactly 90°, only $pd\sigma \times pd\pi$ superexchange processes are allowed, but, since both t_{2g} and e_g states are occupied, their contribution is antiferromagnetic (as opposed to, for instance, Cr^{3+}), and proportional to $t_{pd\sigma}^2 t_{pd\pi}^2/U\Delta^2$, where U is the Hubbard repulsion and Δ is the Mn(d)−Te(π) energy separation. The Goodenough-Kanamori ferromagnetic exchange is of course present, but proportional to $J_H(\mathrm{Te})(t_{pd\sigma}^4 + t_{pd\pi}^4)/\Delta^2$ ($J_H(O)$ being the Hund's rule coupling on Te), which is much smaller.

With this in mind, one may wonder what drives the ferromagnetic order in the planes. The answer is that this is J_3, which is sizable and has high degeneracy of 12, and tries to make the nearest neighbors in the plane of a given Mn antiparallel to the Mn right above, in the neigboring plane, that is, making the nearest neighbors in plane the parallel to each other. It can thus easily overcome the antiferromagnetic J_2.

These findings suggest that the ab domain walls, that is to say, walls perperdicular to the ab plane, should form more easily that those parallel to ab (see Fig. 2). We have verified that through direct density functional (DFT) calculations, using the standard VASP package[11], with the following settings: a 20 formula units supercell, the k-point mesh parallel to the domain boundary 12x12, perpendicular 3, pseudopotentials PAW_PBE Te and Mn_pv, energy cutoff 400 eV, and applying $U - J = 4$ eV, which gives a reasonable direct optical gap of 1.7 eV and indirect gap of 0.8 eV. The results are shown in Table II, where we also show the effect of lattice optimization (positions only). Not unexpectedly, the values are in good agreement with those obtained in the three nearest neighbors model shown in the last line of Table 1, namely 19.4 and 73.9 meV/Mn. Note that all other calculations except the time-consuming structural optimization were performed using the all-electron LAPW package WIEN2k [12], with the same DFT and the same LDA+U setting (although due to different wave function projections the effect of U in these methods is spightlly different). Default WIEN2k settings were used for linearization and cut-offs, and total of 5 different magnetic configurations, each in the minimal supercell, were considered. To avoid systematic errors, for each configuration the difference between the ferro- and antiferro orders was calculated, and only this difference was used for fitting.

TABLE II. Calculated energy of the domain walls, in meV per Mn at boundary.

ab domain		c domain	
not optmized	optimized	not optmized	optimized
19.1	19.0	65.2	55.4

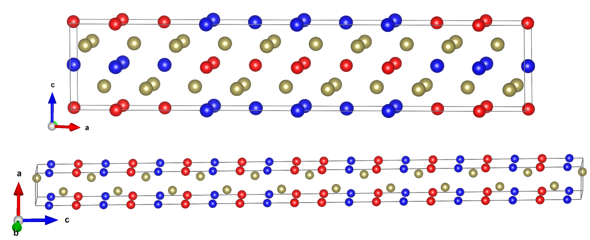

FIG. 2. Supercells used for the domain wall energy calculations for an ab domain (top) and a c domain (bottom). The colors indicate the direction of the Mn sipns (up/down)

As expected, the c wall has a much higher energy and is much less likely to form. On the other hand, since individual ab planes are ferromagnetic, growing MnTe on a single-domain ferromagnetic substrate (with can be easily achieved by applying an in-plane magnetic field) should prevent the ab domains from forming. Numerous antiferromagnets and ferromagnets with stacked ferromagnetic layer with an in-layer easy axis are know, and many have transition temperature above that of MnTe (∼ 310 K), such as[13] $NaOsO_3$ (610 K), (Sc,Ga)FeO_3 (up to 408 K), Fe_2O_3 (960 K), Mn_3(Cu,Ge) (380 K), $FeBO_3$ (348 K), CuMnAs (480 K), but especially promising is $LiMn_6Sn_6$, which in naturally layered, has $T_C \approx 380$ K, and, in addition, has a nearly perfect epitaxial match with MnTe (assuming a $\sqrt{5} \times \sqrt{5}$ superlattice,

$\tilde{a}$ =10.977 Å for the latter and 2×2, $\tilde{a}$ =10.982 Å for the former, a 0.05% match). While epitaxial coherence is not required, it would serve to reduce the distance from the substrate and enhance coupling.

Thus, MnTe is a prime candidate to singe-domain altermagnetism. Unfortunately, it is an insulator, so direct measurement of the anomalous Hall effect is not possible. Fortunately, the altermagnetism there can be probed by magnetooptical tools, such as MOKE (magnetooptical Kerr effect). Also fortunately, the nondiagonal part of the optical conductivity $\sigma_{xy}(\omega)$ can be reliably calculated by modern DFT codes, such as VASP — as opposed to the Hall conductivity, the zero-frequency limit of $\sigma_{xy}(\omega)$, which is impossible to converge in existing calculations, and all current first principle calculations rely upon Wannier-based interpolation, which adds considerable ambiguity. In order to inform the experiments,

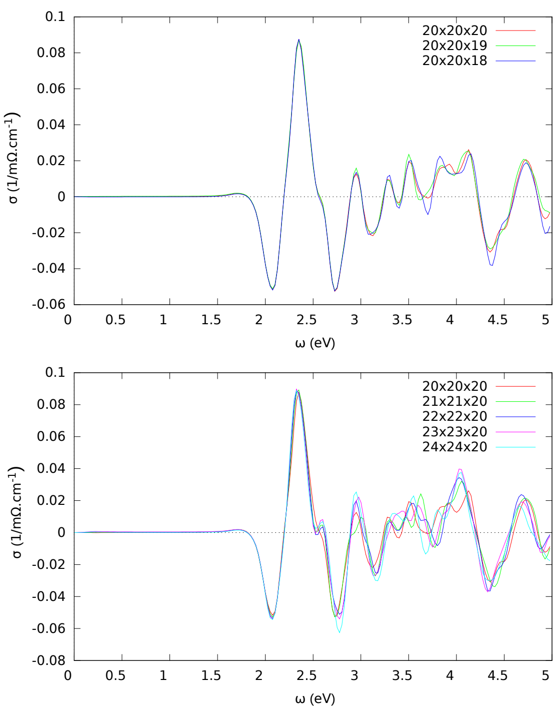

FIG. 3. Calculated nondiagonal optical conductivity σ_{xy}. The two panels show convergence with the respect to the in-plane and out-of-plane k-point mesh, respectively.

which, we hope, will be encouraged by this paper, we have calculated the non-diagonal part of the optical conductivity, for the experimental easy magnetization axis of 210, that is, at $\alpha = 30°$ to the Mn-Mn bond. We show the convergence of $\sigma_{xy}(\omega)$ in Fig. 3. Note that the results are reasonably well converged already at the k-mesh of $20 \times 20 \times 20$; for the Hall conductivity $\sigma_{xy}(0)$ in similar materials an order of magnitude larger linear density is required. Consistent with the symmetry analysis[14], only $\sigma_{xy}(\omega)$ is nonzero, and only for $\alpha \neq 0$. In Fig. 4 we show the angular dependence of $\sigma_{xy}(\omega)/\sin 3\alpha$ as a function of α (due to the hexagonal symemtry, the lowest order term in the angular expansion of $\sigma_{xy}(\omega)$ startes with $\sin 3\alpha$). One can see that the lowest-order expansion holds with a good accuracy.

One should note that, depending on the experiment, various combinations of the elements of the complex dielectric function matrix are measures, and not just σ_{xy}. To this end, in Fig. 5 we show the nonzero components of the function as a function of frequency.

In summary, we (a) explained the microscopic origin of the ferromagnetic ordering in the *ab* plane of MnTe, as driven not by a ferromagnetic in-plane exchange interaction (which has in fact the antiferromagnetic sign), but by the second-interlayer-neighbors antiferromagnetic counplig, (b) computed the energy of the antiferromagnetic domain walls in MnTe, and showed it to be substantial, encouraging growing single-domain samples, where the predicted magnetooptica response can be measured, and (c) calculated the said response and foud it to be sizeable, with a symmetry following the theoretical prediction. We hope that this work will encourage experimental studies of altermagnetism in this compound.

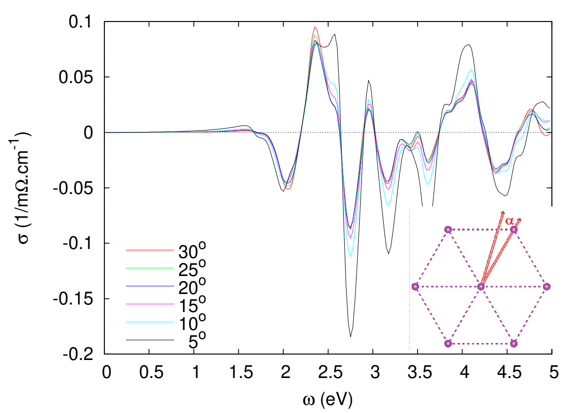

FIG. 4. Dependence of σ_{xy} on the angle α that Mn spins form with Mn-Mn-bond direction (see the inset), divided by $\sin(3\alpha)$.

ACKNOWLEDGMENTS

This research was sponsored by the Army Research Office under Cooperative Agreement Number W911NF-22-2-0173. Some of the images in the paper were created using VESTA software[15].

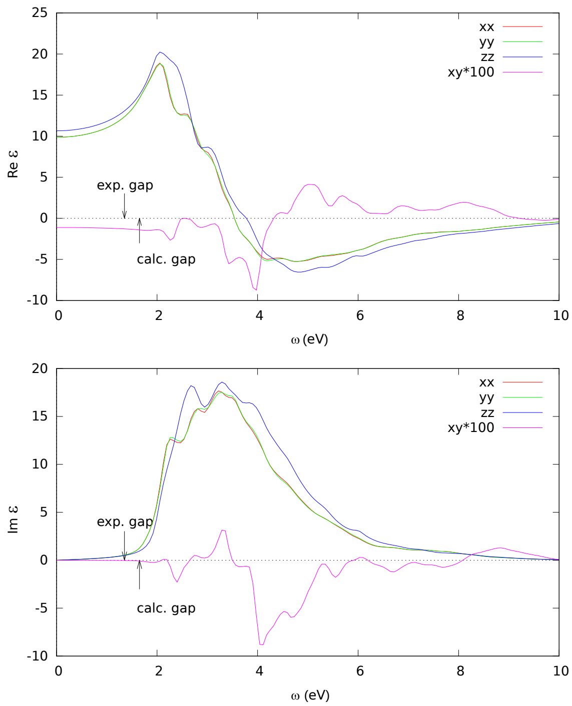

FIG. 5. Calculated complex dielectric function ε_{ij} (i, j are Cartesian indices).

[1] L. Šmejkal, J. Sinova, and T. Jungwirth, Beyond conventional ferromagnetism and antiferromagnetism: A phase with nonrelativistic spin and crystal rotation symmetry, Phys. Rev. X **12**, 031042 (2022).

[2] I. Mazin (The PRX Editors), Editorial: Altermagnetism—a new punch line of fundamental magnetism, Phys. Rev. X **12**, 040002 (2022).

[3] L. Šmejkal, J. Sinova, and T. Jungwirth, Emerging research landscape of altermagnetism, Phys. Rev. X **12**, 040501 (2022).

[4] R. Juza, A. Rabenau, and G. Pascher, Über feste Lösungen in den Systemen ZnS/MnS, ZnSe/MnSe und ZnTe/MnTe, Zeitschrift fr anorganische und allgemeine Chemie **285**, 61 (1956).

[5] C. H. Griffiths, Cubic manganous telluride, Journal of Materials Science **13**, 513 (1978).

[6] D. Kriegner, H. Reichlova, J. Grenzer, W. Schmidt, E. Ressouche, J. Godinho, T. Wagner, S. Y. Martin, A. B. Shick, V. V. Volobuev, G. Springholz, V. Holý, J. Wunderlich, T. Jungwirth, and K. Výborný, Magnetic anisotropy in antiferromagnetic hexagonal MnTe, Phys. Rev. B **96**, 214418 (2017).

[7] W. Szuszkiewicz, E. Dynowska, B. Witkowska, and B. Hennion, Spin-wave measurements on hexagonal MnTe of NiAs-type structure by inelastic neutron scattering, Phys. Rev. B **73**, 104403 (2006).

[8] S. Mu, R. P. Hermann, S. Gorsse, H. Zhao, M. E. Manley, R. S. Fishman, and L. Lindsay, Phonons, magnons, and lattice thermal transport in antiferromagnetic semiconductor mnte, Phys. Rev. Mater. **3**, 025403 (2019).

[9] J. J. Banewicz, R. F. Heidelberg, and A. H. Luxem, High temperature magnetic susceptibilities of MnO, MnSe and MnTe, The Journal of Physical Chemistry **65**, 615 (1961).

[10] T. Komatsubara, M. Murakami, and E. Hirahara, Magnetic properties of manganese telluride single crystals, Journal of the Physical Society of Japan **18**, 356 (1963).

[11] G. Kresse and D. Joubert, From ultrasoft pseudopotentials to the projector augmented-wave method, Phys. Rev. B **59**, 1758 (1999).

[12] P. Blaha, K. Schwarz, G. K. H. Madsen, D. Kvasnicka, and J. Luitz, WIEN2K (2002), ISBN 3-9501031-1-2.

[13] Data for T_N from the Bilbao Crystallographic Server: MAGNDATA — collection of magnetic structures.

[14] L. Šmejkal, R. González-Hernández, T. Jungwirth, and J. Sinova, Crystal time-reversal symmetry breaking and spontaneous Hall effect in collinear antiferromagnets, Science Advances **6**, eaaz8809 (2020), Table 1. (Note that there are two typos in this table: the lower bottom elements in the firts two entries should be σ_{zx}, not σ_{xz}).

[15] K. Momma and F. Izumi, VESTA 3 for three-dimensional visualization of crystal, volumetric and morphology data (2011).